Structural modelling and mechanical tests supporting the design of the ATHENA X-IFU thermal filters and WFI optical blocking filter

Parodi, Giancarlo, D'Anca, Fabio, Lo Cicero, Ugo, Sciortino, Luisa, Rataj, Miroslaw, et al.

Giancarlo Parodi, Fabio D'Anca, Ugo Lo Cicero, Luisa Sciortino, Miroslaw Rataj, Szymon Polak, Adam Pilch, Norbert Meidinger, Kurt Dittrich, Johannes Hartwig, Valérie Samain, Alfonso Collura, Salvatore Ferruggia Bonura, Antonino Buttacavoli, Marco Barbera, "Structural modelling and mechanical tests supporting the design of the ATHENA X-IFU thermal filters and WFI optical blocking filter," Proc. SPIE 10699, Space Telescopes and Instrumentation 2018: Ultraviolet to Gamma Ray, 106994C (6 July 2018); doi: 10.1117/12.2314451

SPIE.

Event: SPIE Astronomical Telescopes + Instrumentation, 2018, Austin, Texas, United States

Structural modeling and mechanical tests supporting the design of the ATHENA X-IFU thermal filters and WFI optical blocking filter

Giancarlo Parodi[a,*], Fabio D'Anca[b,c], Ugo Lo Cicero[c,d], Luisa Sciortino[c], Miroslav Rataj[e], Szimon Polak[e], A. Pilch[f], Norbert Meidinger[g], Kurt Dittrich[g], Johannes Hartwig[g], Valerie Samain[h], Salvatore Varisco[d], Alfonso Collura[d], Salvatore Ferruggia Bonura[c,d], Antonino Buttacavoli[d], and Marco Barbera[c,d]

[a]BCV progetti s.r.l. Milano, IT; [b]Istituto di BioFisica U.O.S. di Palermo – Consiglio Nazionale delle Ricerche, IT; [c]Dipartimento di Fisica e Chimica - Università degli Studi di Palermo, IT; [d]Osservatorio Astronomico di Palermo G. S. Vaiana – Istituto Nazionale di AstroFisica, IT; [e]Space Research Center - Polish Academy of Sciences, Warsaw, PL; [f] Dept. of Mechanics and Vibroacoustics - AGH University, Krakow, PL; [g]Max-Planck-Institut für Extraterrestrische Physik, Garching, DE; [h]Centre Spatial de Liège, Angleur, BE

ABSTRACT

ATHENA is a Large high energy astrophysics space mission selected by ESA in the Cosmic Vision 2015-2025 Science Program. It will be equipped with two interchangeable focal plane detectors: the X-Ray Integral Field Unit (X-IFU) and the Wide Field Imager (WFI). Both detectors require x-ray transparent filters to fully exploit their sensitivity.
In order to maximize the X-ray transparency, filters must be very thin, from a few tens to few hundreds of nm, on the other hand, they must be strong enough to survive the severe launch stresses. In particular, the WFI OBF, being launched in atmospheric pressure, shall also survive acoustic loads.
In this paper, we present a review of the structural modeling performed to assist the ATHENA filters design, the preliminary results from vibration and acoustic tests, and we discuss future activities necessary to consolidate the filters design, before the preliminary requirement review of the ATHENA instruments, scheduled before the end of 2018.

Keywords: Filter, X-Ray, FEA, ATHENA, X-IFU, WFI

1. INTRODUCTION

ATHENA (Advanced Telescope for High-Energy Astrophysics) is a Large-class astrophysics space mission, selected by ESA in the Cosmic Vision 2015-2025 Science Program and due for launch by 2030[1]. ATHENA will be equipped with an X-ray telescope with a focal length of 12 m and two interchangeable focal plane detectors: the X-ray Integral Field Unit (X-IFU)[2], an array of micro-calorimeters, and the Wide Field Imager (WFI)[3], a large array of depleted field effect transistors (DEPFET). Both detectors require X-ray transparent filters to fully exploit their sensitivity. The X-IFU, operating at temperatures below 100 mK inside a cryostat, requires a set of thermal filters (TF) to reflect infrared (IR) radiative load, protect the detector from molecular contamination and attenuate RF from the satellite telemetry. The WFI requires an optical blocking filter (OBF), which will be mounted on a filter wheel[4], to reduce the optical load from bright ultraviolet/visible (UV/VIS) astrophysical sources.

In order to maximize the X-ray transparency, filters must be very thin, from few tens to few hundreds of nanometers, and made of light materials, typically a polymer coated with a low Z metal such as aluminum. On the other hand, such filters must be strong enough to survive the severe launch stresses. The X-IFU filters, being launched in vacuum, shall survive static pressure load, occurring for example during vacuum-venting procedures, shock and vibrations. The WFI OBF, being launched in atmospheric pressure, shall also survive acoustic loads.

* giancarlo.parodi@bcv.it; phone +39 02 86452002; BCV progetti Srl, via Sant'Orsola 1, I 20123 Milano.

Space Telescopes and Instrumentation 2018: Ultraviolet to Gamma Ray, edited by Jan-Willem A. den Herder, Shouleh Nikzad, Kazuhiro Nakazawa, Proc. of SPIE Vol. 10699, 106994C · © 2018 SPIE
CCC code: 0277-786X/18/$18 · doi: 10.1117/12.2314451

Large size filters, made by a sub-micron thick polyimide carrier coated with aluminum, have been used in several recent missions such as Chandra[5][6] and XMM-Newton[7], demonstrating reliability and long-term stability. For instance, the 75 mm diameter thin filters of the EPIC camera on board XMM-Newton consist of an unsupported 120 nm thick polyimide film, coated with 40 nm of aluminum. Such filters survived launch loads and are still working with no clear sign of degradation[8][9]. Such positive heritages suggested to consider polyimide carrier coated with aluminum as baseline for the WFI OBF and for the X-IFU TFs. The large size of the filters and the high load levels, particularly for acoustic loads on WFI OBF, also suggested to adopt supporting metallic meshes, glued to the polyimide film. Hereafter, we do not get into optical and thermal filter performances[10][11], but we focus on filter structural design, numerical modeling and mechanical tests.

2. CURRENT DESIGN DATA

2.1 Filter geometries

The X-IFU baseline is to use five thermal filters (TF) mounted in the windows opened on the cryostat that contains the sensors. They attenuate the IR radiative load and the Radio Frequency (RF) electromagnetic interference coming from onboard electronics and from telemetry antenna onto detector[12][13].

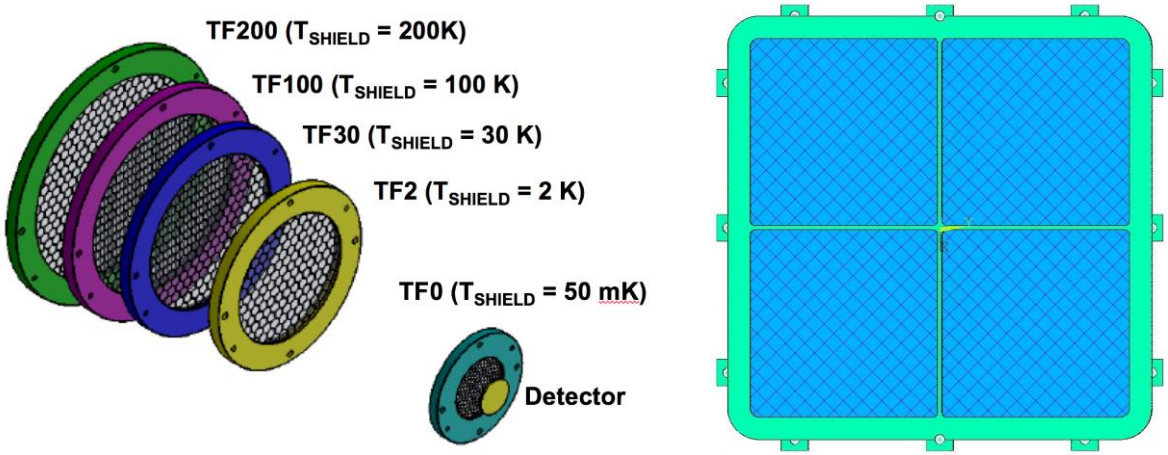

Figure 1. Schematic layout of the X-IFU thermal filters (left) and the WFI Large Detector Array (LDA) OBF (right).

According to the current design all X-IFU TFs are circular, with diameter ranging from 26 mm to 100 mm, and distance from the focal plane from 15 mm to 240 mm. They consist of polyimide foils 45 nm thick, with a 30 nm aluminum coating. Metallic meshes provide support to such thin membranes offering also RF attenuation up to 20 GHz[13]. Current design envisages SAE 304 stainless steel (SS) meshes, with the sole exception of the filter nearest to the detector array, where a niobium mesh is under investigation.

Table 1. X-IFU TF geometry and operating temperatures.

Filter Name	Diameter [mm]	Polyimide thickness [nm]	Aluminum thickness [nm]	Distance from detector [mm]	Operating temperature [K]
TF0	26	45	30	15	0.05
TF2	56	45	30	150	2
TF30	76	45	30	180	30
TF100	88	45	30	210	100
TF200	100	45	30	240	200

Metallic supporting meshes have hexagonal cells. Their geometry is characterized by the wire cross section and by the pitch, i.e. the distance between the center of two adjacent cells. Table 2 summarizes mesh data relevant to the smallest and largest X-IFU TFs. We have to point out that, due to technological manufacturing constraints, the maximum ratio achievable between wire thickness and wire width is 2. It is clear that in principle higher ratio could help in reducing the geometrical blocking factor, defined as the ratio between the area occupied by mesh and the aperture area.

Table 2. X-IFU TF: Metallic mesh geometry.

Filter Name	Mesh material	Pitch [mm]	Wire width [µm]	Wire thickness [µm]	Blocking factor
TF0	Nb	2	30	60	~ 4%
TF300	SAE 304 SS	5	65	130	~ 3%

The WFI large detector array (LDA) OBF is square shaped, 170 mm × 170 mm. SS supporting mesh, having square layout parallel to filter diagonals, has been used in consideration of the very large size. A cross shaped stiffening frame divides the WFI OBF in four equal sub-apertures (see Figure 1 right). Main geometrical data are summarized in table 3.

Table 3. WFI large detector array OBF geometry.

Filter Name	Size [mm^2]	Polyimide thickness [nm]	Aluminum thickness [nm]	Mesh pitch [mm]	Wire width [µm]	Wire thickness [µm]	Blocking factor
WFI OBF	170×170	150	30	6	100	200	~ 3.5%

2.2 Material mechanical properties

Mechanical properties of materials are summarized in table 4. No structural contribution has been assigned to aluminum coating, considered just as a mass, likewise the 5 µm thick gold coating on the supporting metallic meshes.

Table 4. Room temperature mechanical properties of the materials.

Material	Density [t/m^3]	Young modulus [GPa]	Poisson ratio	Elastic limit [MPa]	Ultimate tensile strength [MPa]	Coefficient of Thermal Expansion [K^{-1}]
LUXFilm® polyimide	1.41-1.47	6.9	NA[1)]	70[2)]	310	3×10^{-6}
SAE 304 stainless steel	8	200	0.3	NA	1142[3)]	16×10^{-6}
Niobium	8.6	103	0.38	200	330	7×10^{-6}
Al alloy[4)]	2.9	68	0.36	480	540	24×10^{-6}

1) Poisson ratio equal to 0.35 has been used in Finite Element Analysis.
2) Bhandarkar S., et al. (2016)[14]
3) Manufacturer data.
4) WFI and X-IFU frames.

2.3 Current reference load levels at launch

Assessment of filter interface load levels at launch have still to be finalized. Nevertheless, we report hereafter reference values, used in mechanical vibration and shock tests carried out so far. Table 5 reports the sine (0-peak amplitude level) and random vibration (Power Spectral Density) test reference spectra. Shock response spectrum having 400 g plateau between 1000 and 3000 Hz, with the ramp defined by 20 g at 100 Hz has been used for tests.

Table 5. Sine and random vibration reference levels.

SINE VIBRATION		**RANDOM VIBRATION**	
Frequency Range [Hz]	**Level**	**Frequency Range [Hz]**	**PSD**
5.0 - 24.1	9.9 mm (0-peak)	20 - 100	+3 dB/Oct.
24.1 - 26.2	1.5 m/s (0-peak)	100 - 300	0.5 g^2/Hz
26.2 - 100	25 g (0-peak)	300 - 2000	-5 dB/Oct.
Sweep rate 2 Oct/min		**16.9 g RMS - Duration 150s**	

With regards to the acoustic loads applied to WFI OBF. the qualification level of ARIANE V[15] has been used during tests. The overall level of acoustic pressure is 139.5 dB with 2 minutes duration.

3. STRUCTURAL DESIGN AND NUMERICAL MODELING

The filters structural design is supported by numerical modeling activities carried out using the ANSYS Mechanical software. We have to remind that the possibility to achieve reliable results from numerical modeling is affected in this case by several factors; just to mention the main ones:

- Non-linearity + concurrent random loads. Geometrical non-linearity is related to membrane structural behavior of both the film and the mesh. Right at the mesh edges, fixed to the outer mounting frame, bending stress in the mesh wires prevail, giving rise to the maximum stress peaks. The visco-elastic film is affected by material non-linearity, while for design purposes the mesh is considered still elastic under maximum load levels.
- Lack of any membrane pre-stress, giving an initial stiffness to the film.
- Local random deformations (see Figure 2) in the film, as detected in the first samples realized so far.
- Film stress concentration factors (SCF), due to potential local defects (pin holes, small irregularities of the film-mesh adhesive connection, if any) to be quantified.
- Lack of knowledge of some film mechanical properties (for instance strength under cyclic loads).

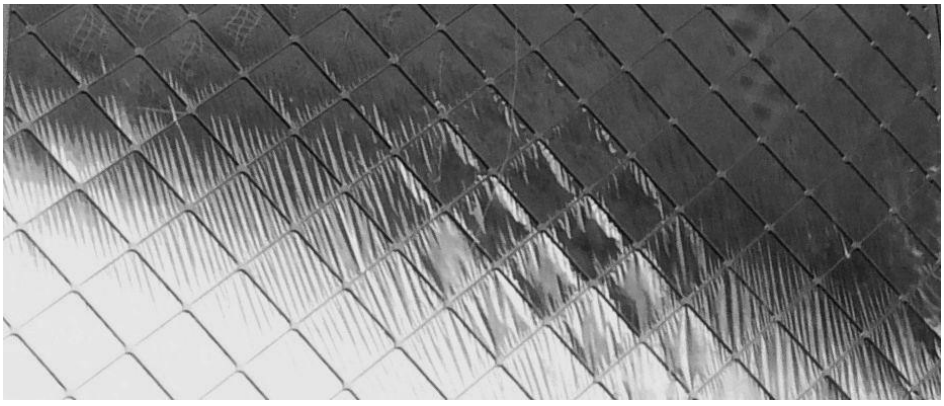

Figure 2.WFI OBF sample at delivery condition before any load tests. The film inside each cell shows wrinkles and some random deformations, impacting on the structural local response to applied load. The occurrence of possible defects at the interface where the film is glued to the mesh is not clear.

It is clear that in such conditions experimental tests become the ultimate and decisive criteria to validate any filter design. Nevertheless, numerical modeling is still useful to address the design phase and the experimental test interpretation, to identify possible criticalities in the film, to compare different film/mesh configurations, and to provide stress and deformation prediction for the meshes.

Well aware of the criticalities mentioned above, some numerical analyses underlying the preliminary filter design have been carried out according to the following criteria:

- Nominal geometry, no local shape randomness and no pre-stress or defects in the film/mesh have been accounted for. At the same time the assessment of the impact on stress peaks due to possible film defects has been carried out.
- Non-linear analyses under static uniform pressure. 10 mbar has been used as reference level of differential pressure between the two filter sides. Such value was derived from qualification level for Newton-XMM EPIC filters[7] and from some rough and preliminary assessment of the static pressure "equivalent" to WFI OBF acoustic loads. Such value was then reduced for X-IFU filters, which are not subject to acoustic loads.
- Maximum mesh stress < 0.5×ultimate tensile strength (~ 570 MPa for SS, and 165 MPa for Nb).
- Maximum principal tensile stress in the film <70-80 MPa. According to Bhandarkar et al.[14] it seems reasonable to still consider the film elastic at this stress level. Elastic-plastic materials have been used in finite element analysis (FEA) with elastic limit at 70 MPa[14].

Main preliminary design activities are briefly summarized hereafter.

3.1 Step 1 - Stress in the polyimide film

At first, parametric analyses of the principal tensile stress in the film under static differential pressure vs. thickness (dictated by optical requirements), size, and shape of the mesh cell have been carried out. At this step, just one single elementary cell, rigidly supported along the edges, with nominal shape, has been considered. Some examples of the achieved results are shown in Figure 3.

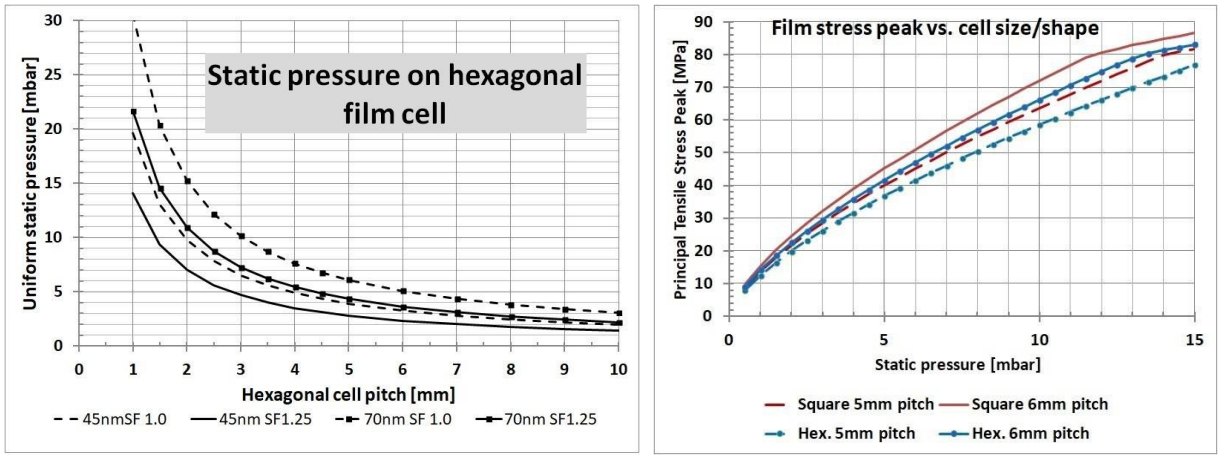

Figure 3. The plot on the left shows the maximum static pressure that a polyimide film can withstand before permanent deformation occurs, as a function of the hexagonal cell pitch and film thickness (45-70 nm). Two values of the safety factor (SF) on the elastic limit are considered (SF = 1.0 and SF = 1.25). The plot on the right shows the tensile stress peak in a polyimide film 150 nm thick as a function of the applied static pressure for two different cell sizes (5 mm vs. 6 mm) and shapes (square vs. hexagonal).

Then the elastic stress concentration factors (SCF) for different hypothetical defects in the film body (pin hole) or at the glued interface with the mesh wires have been computed.

As it is well known[16], SCF related to pin holes is equal 3. Defects at film/mesh interface, if any, are not quantified. Performed analyses pointed out the risk of having very high SCF in case of defects at film/mesh interface (Figure 4).

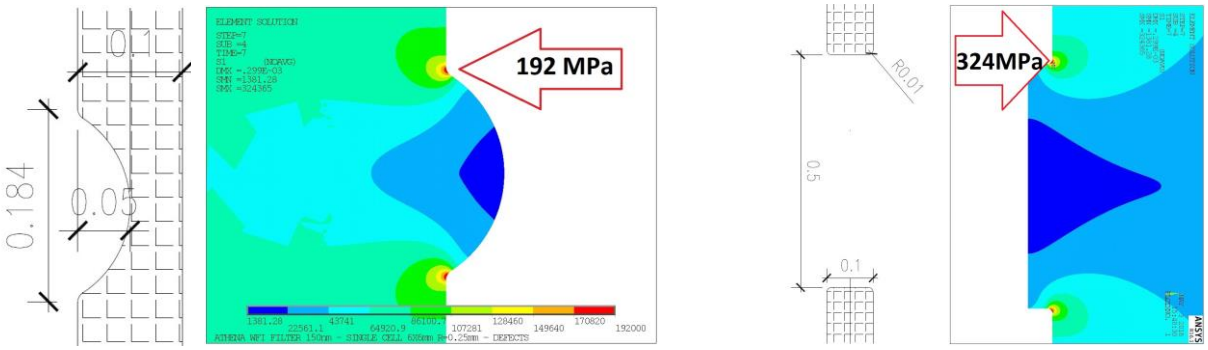

Figure 4. Example of film/mesh interface defects (dimension in millimiters) and correspondent stress peak under 10 mbar pressure vs. the nominal stress, without defects, equal to 72 MPa. The picture on the left shows the film stress peak in case the adhesive fillet (100 μm wide) connecting the film to the mesh is missed on a spot 184 μm long and 50 μm wide. The picture on the right is relevant to an adhesive fillet disruption 500 μm long.

3.2 Step 2 - Mesh design and filter trade-off

The behavior in terms of deflections and stress peaks of different mesh layouts (see Figure 5), different wire materials and wire cross sections under 10 mbar static pressure has been analyzed for the different filters.

At the same time, the structural performances of different filter shapes have been compared for WFI OBF: a square filter performs relatively better than a circular one and, above all, taking advantage of the thin dead zone between the four detector modules (quadrants), it easily allows the integration of a central cross frame stiffener (see Figure 1, right). The cross actually, from the structural point of view, turns the 170 mm × 170 mm filter in four 84 mm × 84 mm filters[10] (see Figure 6, left).

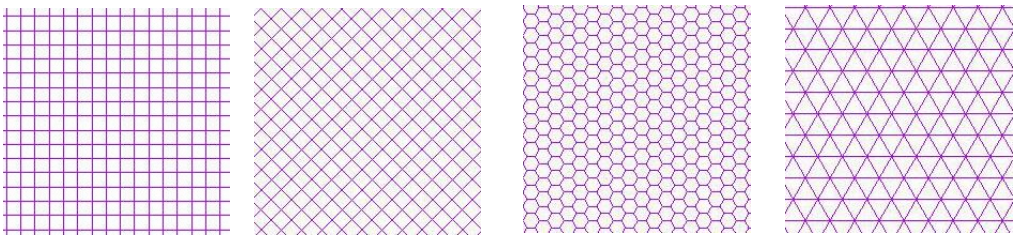

Figure 5. Investigated mesh layouts (left to right): square, 45° rotated square, hexagonal, triangular. Independently on the mesh pattern used, the same geometrical blocking factor is achieved, provided that the same wire width and the same distance between elementary cell centers is used.

The preliminary trade-off analysis, mainly focused on the WFI imaging detector OBF and on the largest and the smallest X-IFU TFs, has been carried out on the basis of results derived from steps 1 and 2, producing the design parameters already summarized in tables 2-3.

Analyses of the assembly composed by mesh + film + outer frame, considered screwed to a rigid interface, confirmed stress levels derived at step 1 from the single cell analysis, as proof that film stresses are mainly affected by local membrane behavior inside each elementary cell. Clearly, also the global filter deformation has some impact on film stress, but to a much lesser degree (see Figure 6, right).

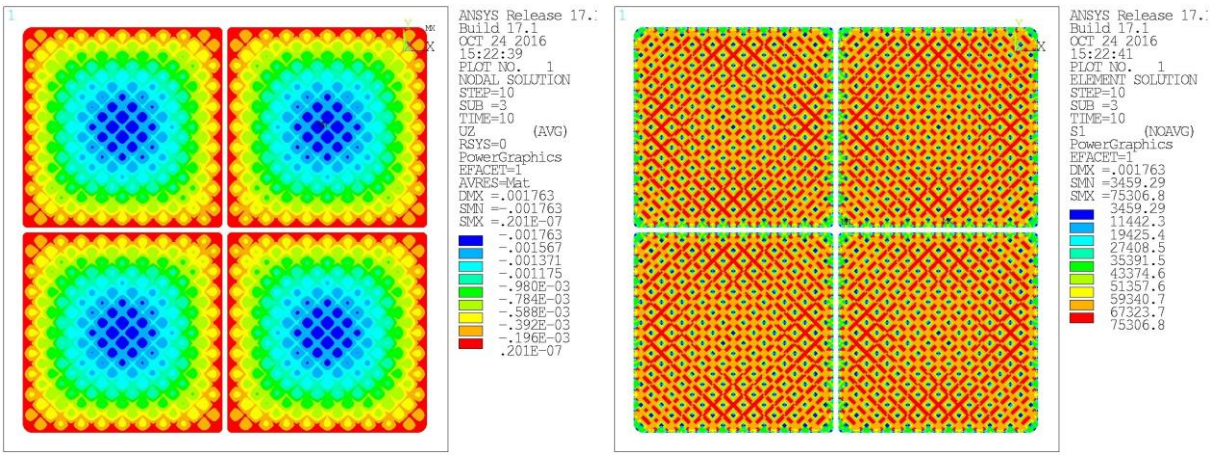

Figure 6. WFI OBF loaded with 10 mbar static pressure. Picture on the left shows the deformation contours quoted in meters (max. deformation = 1.76 mm). Picture on the right shows the principal tensile stress in the film quoted in kilopascal (max. stress = 75.3 MPa).

3.3 Frequency assessment

The lowest resonance frequency, derived from numerical modeling, computed in vacuum and for the un-deformed filter, is approximately 91 Hz for the WFI LDA OBF.

For a filter having the same mesh of X-IFU TF200, but with a smaller diameter of 85 mm (Figure 7) instead of 100 mm, 80 Hz has been computed (see Table 2). Since in circular plates the resonance frequency is inversely proportional to the squared radius, a 58 Hz resonance frequency is expected for X-IFU T200. It is worth recalling that since filters are not preloaded there is no film contribution to the filter stiffness, all the stiffness is due to the mesh (just bending stiffness when the filter is un-deformed).

Frequency values mentioned above are definitely low, falling in the sine vibration range (see table 5), but there is few margin to significantly increase them, since an increase of the mesh wire width (or the pitch reduction) would entail larger blocking factor, while an increase of the mesh wire thickness is not allowed, since we already used the maximum thickness compliant with technological constraints (thickness/width ≤ 2).

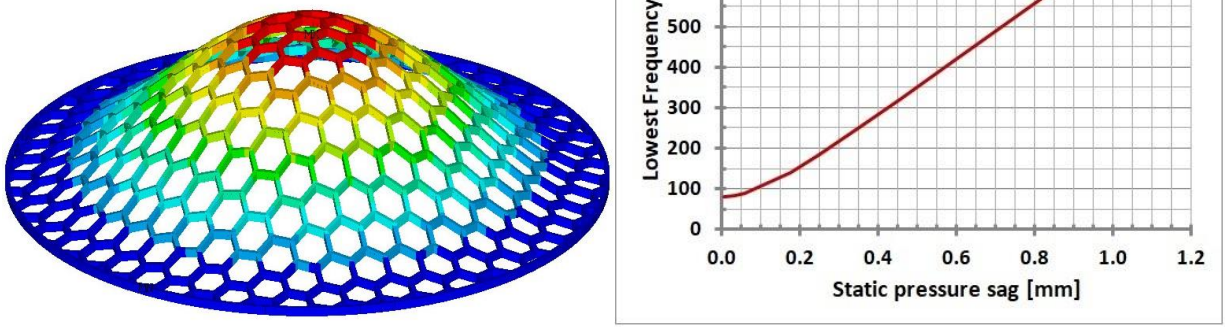

Figure 7. Circular filter Ø 85 mm, 5 mm pitch hexagonal mesh, 65 µm × 130 µm (width×thickness) wire – First modal shape (left). Lowest mode frequency as a function of the sag (and consequent membrane stresses) produced by static uniform pressure (right).

On the other hand, we have to remember that the above frequencies values, related to the un-deformed filter, would keep their significance only if the structural behavior were linear. On the contrary, the filter behavior is strongly non-linear due to membrane stiffening effects, so the frequency values stated above become meaningless as soon as the small displacement hypothesis loses its validity. Figure 7 (right) points out that under uniform pressure, giving 0.1 mm sag, the frequency is 25% higher respect to un-deformed condition.

Due to the structural non-linearity, frequency values in the sine vibration range lose most of their hazard. Even at "resonance" the filter vibration amplitude is significantly capped by the membrane stiffening, even with a structure having such a low damping.

Such behavior is well highlighted in Figure 8. Here the out of plane accelerations of three points at the filter centre, at intermediate radius and at the outer edge are reported when 0.5 g out-of-plane sine acceleration is applied at the outer edge. The frequency of the applied acceleration is 80 Hz, exactly in resonance with the first filter frequency. Damping ratio is equal to 0.005.

Picture on the left is computed in the hypothesis of linear system, neglecting the membrane stiffening which, on the contrary, is taken into account in the picture on the right. The comparison of the first few cycles points out the larger and erroneous magnification factor computed by linear approach.

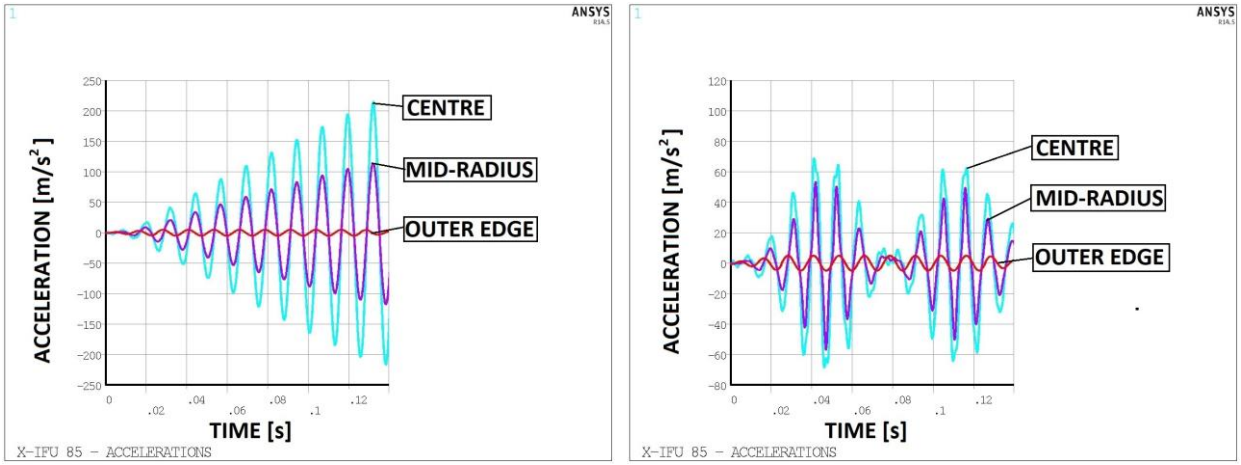

Figure 8. Circular filter Ø 85 mm, 5 mm pitch hexagonal mesh, 65 μm × 130 μm (width×thickness) wire – Acceleration time history for 0.5 g sinus acceleration at the outer edge (80 Hz); linear analysis without membrane stiffening (left); non-linear analysis with membrane stiffening (right).

4. MECHANICAL TESTS

Filter samples, fabricated according to designs reported in tables 1 to 3, have been submitted to vibration, shock and acoustic tests.

First test campaigns were mainly focused on the metallic meshes so, due to economic reasons, the polyimide film was replaced by a thicker polypropylene membrane (thickness < 1 μm). During vibration test sessions held at Centre Spatiale de Liège (March 2017) and at Max-Planck-Institut für Extraterrestrische Physik (MPE, Garching, November 2017) SS and Nb meshes survived to the shock load (400 g) and to vibration levels higher than those reported in Table 5: 35g for sine, +3 dB for random (23.9 g RMS)[17].

Same load levels have been successfully applied to one quadrant (84 mm × 84 mm) of the WFI OBF prototype, with nominal 150 nm thick polyimide film, tested during MPE campaign in Nov. 2017.

SS mesh of WFI imaging detector OBF survived also ARIANE V qualification acoustic loads (Figure 9) during tests held on May 2017 at University of Science and Technology (AGH University) - Dept. of Mechanics and Vibro-Acoustics, Krakow. Also in this case polyimide was replaced by polypropylene film having thickness < 1μm.

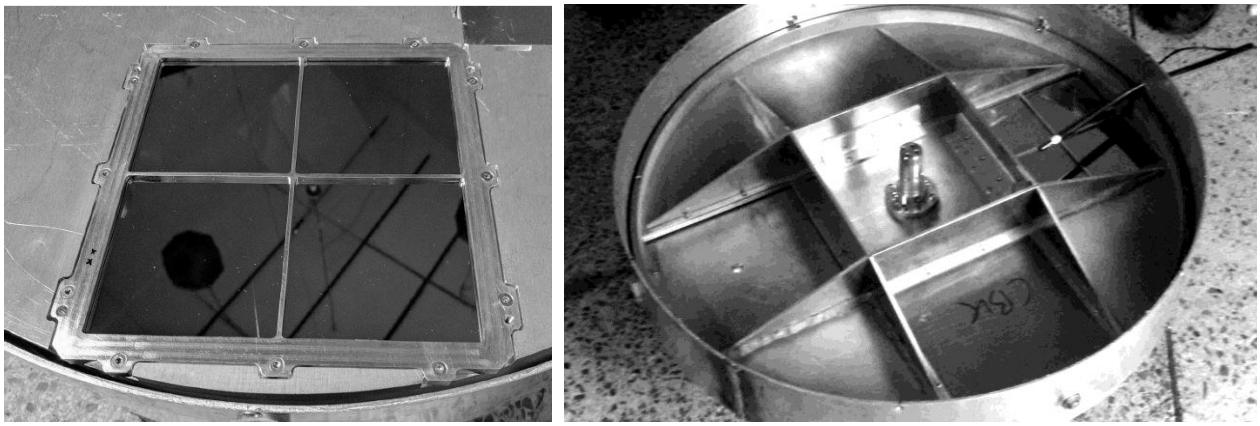

Figure 9. WFI OBF filter during acoustic tests at AGH University on May 2017 (left). The filter was mounted in filter wheel mock-up to simulate the effective acoustic levels (right).

Later on April 2018 one quadrant (84 mm × 84 mm aperture) of the WFI OBF with polyimide film has been tested for acoustic load at AGH University using a filter wheel mock up and the ARIANE V acoustic load at qualification level (Figure 10, left). During tests polyimide film showed local failures in some cells, see Figure 10 (right).

Figure 10. WFI OBF filter during acoustic tests at AGH University on April 2018. Filter wheel mock-up (left). Film failures at the test end (right). The metallic mesh stopped the propagation of the failures to the whole film.

Remedy measures are under assessment; they consist in:

a) film stress reduction, if necessary, by changing the cell shape from square to hexagonal and/or the cell pitch. Figure 3 (right) points out the improvements achievable by reducing the pitch and/or the cell shape.
b) assessment by analysis of the impact due to potential sources of overstresses in the film (film wrinkles as those shown in Figure 2, which actually refer to the failed film in Figure 10 and SCF at film-mesh interface) based on a technical discussion with the manufacturer to identify and, if possible, to reduce any potential overstress sources.

It must be noted that, due to constraints imposed by optical requirements, a moderate stress reduction can be expected from point a) while more dangerous overstresses could be related to topics in point b).

5. FUTURE PERSPECTIVES

Future activities should be aimed to the:

- definition of the filter designs, overcoming the criticalities occurred during test campaigns carried out so far.
- Design validation by tests on the basis of environmental load levels, derived from instrument design. Tests shall also include thermo-vacuum and thermal cycling tests.
- Improvement of the numerical modeling reliability.

To improve the reliability of structural filter modeling, the following actions are envisaged:

- Proper test program to acquire deeper knowledge of the filter behavior to be compared with structural model results, by measuring the deformation under static pressure.
- The possibility to measure filter frequencies and deformed shapes under dynamic loads by laser scanner vibrometer, that is under assessment at MPE (see Figure 11).

Finally, we stress once more the hope that the improvement of the film configuration inside each cell will be possible, avoiding wrinkles and any severe overstress sources.

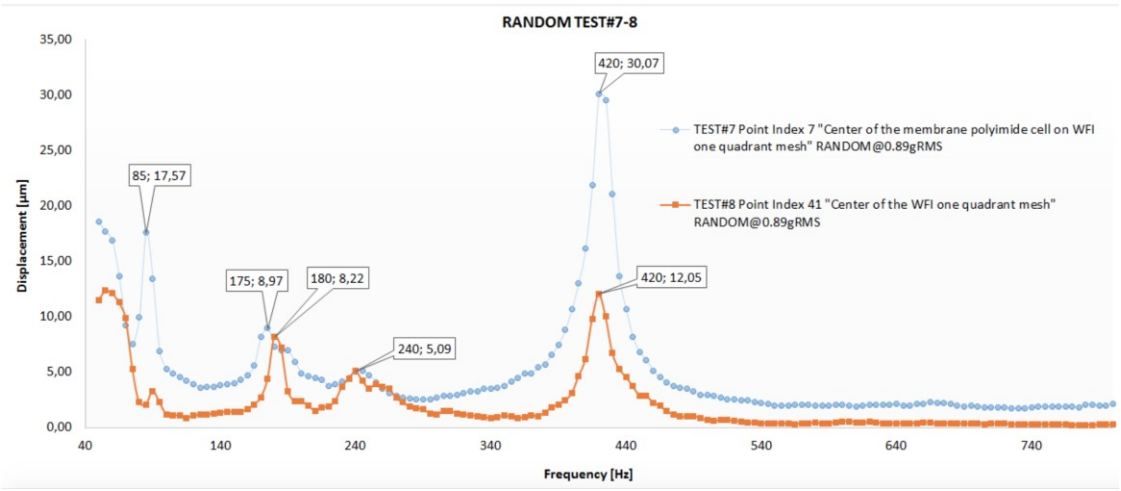

Figure 11. WFI OBF filter – Spectrograms of two points at the centre of one quadrant, obtained by low level random vibration test (0.89 g RMS). Red curve refers to a point on the metallic mesh, while blue curve is relevant to a point at the centre of one cell. Lowest frequencies confirm quite well numerical results (91 Hz and 180 Hz for the mesh). The 420 Hz peak is due to the mechanical jig used to mount the filter.

ACKNOWLEDGEMENTS

The research leading to these results has received funding from ASI (Italian Space Agency) under the contract n. 2015-046-R.0, from the European Union's Horizon 2020 Program under the AHEAD project (grant agreement n. 654215), and from ESA (European Space Agency) under the contract n. 4000120250/17/NL/BJ. We acknowledge fruitful discussions and support by LUXEL corp. We also acknowledge fruitful discussions and suggestions by Josef Eder of MPE.

REFERENCES

[1] Barcons, X., et al., "Athena: the X-ray observatory to study the hot and energetic Universe", Journal of Physics Conference Series, Volume 610, Issue 1, (2015). doi:10.1088/1742-6596/610/1/012008

[2] Barret, D., et al., “The ATHENA X-ray Integral Field Unit (X-IFU)”, Proc. SPIE 9905, 99052F-1, (2016). doi: 10.1117/12.223243
[3] Meidinger, N. et al., “The Wide Field Imager instrument for Athena”, Proc. SPIE 10397, 103970V, (2017). doi: 10.1117/12.2271844
[4] Rataj, M., et al., “The filter and calibration wheel for the ATHENA wide field imager”, Proc. SPIE 9905, 990568, (2016). doi: 10.1117/12.2235411
[5] Barbera M., Austin K., Collura A., Flanagan A., Jelinsky R., Murray S., Serio S., Zombeck M., "Development of the UV/ion shields for the Advanced X-ray Astrophysics Facility high-resolution camera (AXAF HRC)", Proc. SPIE 2280, 214-228 (1994). doi: 10.1117/12.186815
[6] Meehan R., Murray S., Zombeck V., Kraft P., Kobayashi K., Chappell H., Kenter T., Barbera M., Collura A., Serio S., "Calibration of the UV/ion shields for the AXAF High-Resolution Camera", Proc. SPIE 3114, 74-100 (1997). doi: 10.1117/12.283790
[7] Villa G.E., Barbera M., Collura A., La Palombara N., Musso C., Serio S., Stillwell R., Tognon P., Turner D.C., “The optical/UV filters for the EPIC experiment”, IEEE Trans. on Nuclear Science, 45, 921-926 (1998).
[8] Barbera M., Agnello S., Buscarino G., Collura A., Gastaldello F., La Palombara N., Lo Cicero U., Tiengo A., Sciortino L., Varisco S., Venezia A. M., "Status of the EPIC thin and medium filters on-board XMM-Newton after more than 10 years of operation: 1) laboratory measurements on back-up filters", Proc. SPIE 8859, 885914 12 pp. (2013). doi: 10.1117/12.2030896
[9] Gastaldello F., Barbera M., Collura A., La Palombara N., Lo Cicero U., Sartore N., Tiengo A., Varisco S., "Status of the EPIC thin and medium filters on-board XMM-Newton after more than 10 years of operation: 2) analysis of in-flight data", Proc. SPIE 8859, 885915 6 pp. (2013). doi: 10.1117/12.2030897
[10] Barbera M., Branduardi-Raymont G., Collura A., Comastri A., Eder J., Kamisiński T., Lo Cicero U., Meidinger N., Mineo T., Molendi S., Parodi G., Pilch A., Piro L., Rataj M., Rauw G., Sciortino L., Waver P., “The optical blocking filter for the ATHENA Wide Field Imager: ongoing activities towards the conceptual design”, Proc. SPIE Vol. 9601, 960109, (2015). doi: 10.1117/12.2189326
[11] Barbera M., Argan A., Bozzo E., Branduardi-Raymont G., Ciaravella A., Collura A., Cuttaia F., Gatti F., Jimenez Escobar A., Lo Cicero U., Lotti S., Macculi C., Mineo T., Nuzzo F., Paltani S., Parodi G., Piro L., Rauw G., Sciortino L., Sciortino S., Villa F., “Thermal filters for the ATHENA XIFU: ongoing activities towards the conceptual design”, J. Low Temp. Phys. 184, 706–711, (2016). doi: 10.1007/s10909-016-1501-4
[12] Barbera et al., “Development status of the ATHENA X-IFU thermal filters toward the end of phase A,” Proc. SPIE, 10699, in press (2018).
[13] Lo Cicero U., et al., “Radio Frequency shielding of thin aluminized plastic filters investigated for the ATHENA X-IFU detector”, Proc. SPIE, 10699, in press (2018).
[14] Bhandarkar S., Betcher J., Smith R., Lairson B., Ayers T., “Constitutive models for the viscoelastic behavior of polyimide membranes at room and deep cryogenic temperatures”, Fusion Science and Technology, Vol. 70, 332-340, (2016). dx.doi.org/10.13182/FST15-218
[15] ARIANESPACE, “Ariane 5 User’s Manual”, Issue 5 Revision 2 (Oct. 2016).
[16] Young W. C., Budynas R. G., “Roark’s Formulas for Stress and Strain”, McGraw Hill, 7th ed., (2002).
[17] Barbera, M., et al., “Preliminary Mechanical Characterization of Thermal Filters for the X-IFU Instrument on Athena”, JLTP published on-line, (2018). doi: https://doi.org/10.1007/s10909-018-1942-z